

© 2024 IEEE. Personal use of this material is permitted. Permission from IEEE must be obtained for all other uses, in any current or future media, including reprinting/republishing this material for advertising or promotional purposes, creating new collective works, for resale or redistribution to servers or lists, or reuse of any copyrighted component of this work in other works.

# DAVIS-Ag: A Synthetic Plant Dataset for Prototyping Domain-Inspired Active Vision in Agricultural Robots

Taeyeong Choi<sup>1</sup>, Dario Guevara<sup>2</sup>, Zifei Cheng<sup>3</sup>, Grisha Bandodkar<sup>3</sup>,  
Chonghan Wang<sup>3</sup>, Brian N. Bailey<sup>4</sup>, Mason Earles<sup>2,5</sup>, and Xin Liu<sup>3</sup>

**Abstract**—In agricultural environments, viewpoint planning can be a critical functionality for a robot with visual sensors to obtain informative observations of objects of interest (e.g., fruits) from complex structures of plant with random occlusions. Although recent studies on active vision have shown some potential for agricultural tasks, each model has been designed and validated on a unique environment that would not easily be replicated for benchmarking novel methods being developed later. In this paper, we introduce a dataset, so-called DAVIS-Ag, for promoting more extensive research on Domain-inspired Active VISION in Agriculture. To be specific, we leveraged our open-source “AgML” framework and 3D plant simulator of “Helios” to produce 502K RGB images from 30K densely sampled spatial locations in 632 synthetic orchards. Moreover, plant environments of strawberries, tomatoes, and grapes are considered at two different scales (i.e., Single-Plant and Multi-Plant). Useful labels are also provided for each image, including (1) bounding boxes and (2) instance segmentation masks for all identifiable fruits, and also (3) pointers to other images of the viewpoints that are *reachable* by an execution of action so as to simulate active viewpoint selections at each time step. Using DAVIS-Ag, we visualize motivating examples where fruit visibility can dramatically change depending on the pose of the camera view primarily due to occlusions by other components, such as leaves. Furthermore, we present several baseline models with experiment results for benchmarking in the task of target visibility maximization. Transferability to real strawberry environments is also investigated to demonstrate the feasibility of using the dataset for prototyping real-world solutions. For future research, our dataset is made publicly available online: <https://github.com/ctyeong/DAVIS-Ag>.

## I. INTRODUCTION

For precision agriculture, accurate perception is an essential functionality for robots to identify the maturity or health statuses of plants. One of the challenges is, however, caused by the wild environments, in which various objects such as fruits, stems, and leaves can be only partially visible due to occlusions by one another [1]. For instance, a diseased fruit could be more easily misclassified as a normal instance when the anomalous parts are not fully visible [2]. In addition, yield estimation can be inaccurate, if a crop detector cannot access the views to some of occluded individuals [3].

As a potential solution, “active vision” approaches [4] have recently been developed, in which an embodied agent plans its motion sequence to gain more informative viewpoints

<sup>1</sup>Department of Information Technology at Kennesaw State University, USA, <sup>2</sup>Department of Viticulture and Enology, <sup>3</sup>Department of Computer Science, <sup>4</sup>Department of Plant Sciences, and <sup>5</sup>Department of Biological and Agricultural Engineering at the University of California, Davis, USA. [tchoi3@kennesaw.edu](mailto:tchoi3@kennesaw.edu),  [{dguevara, zfcheng, gbandodkar, wchwang, bnbailey, jmearles, xinliu}@udcavis.edu](mailto:{dguevara, zfcheng, gbandodkar, wchwang, bnbailey, jmearles, xinliu}@udcavis.edu)

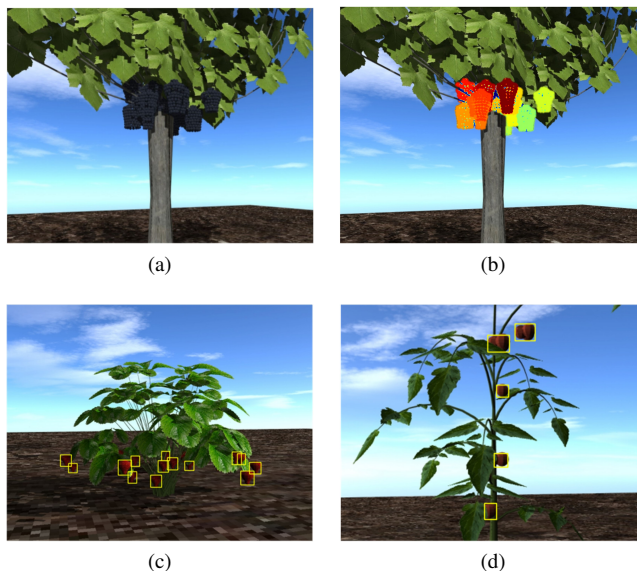


Fig. 1: Example images from single-plant scenarios of DAVIS-Ag: (a)–(b) goblet vine, (c) strawberry, and (d) tomato. Labels for fruits are also visualized with bounding boxes in (c)–(d), and instance segmentation of (a) in (b).

around plants. More specifically, a robotic arm with some camera sensor on it is often deployed to move effectively while maximizing the area coverage of fruit to potentially classify its maturity [5], [6], predict the size and pose information [7], or reconstruct its complete 3D structures [8], [9], [10]. However, every model has been built up on a uniquely customized environment within either simulation or physical setups that could not be easily replicated without technical familiarity when new studies try to benchmark their novel approaches.

To bridge this gap, in this paper, we introduce an easy-to-access dataset, so-called **Domain-inspired Active VISION in Agriculture (DAVIS-Ag)**, which contains over 502K HD-quality RGB images gathered from 30K sampling locations with diverse viewpoints around realistically simulated plants under varying phenotypic parameters (cf. Fig. 1 and Fig. 6h–6j). Specifically, 634 synthetic orchards of strawberries, tomatoes, and grapes are considered at two different scales (i.e., Single-Plant and Multi-Plant). Moreover, unlike typical agricultural image datasets [11], DAVIS-Ag provides the “pointers” between reachable viewpoints by possible actions (i.e., *forward*, *backward*, *left*, *right*, *rotate*, *up*, *down*, etc.) to

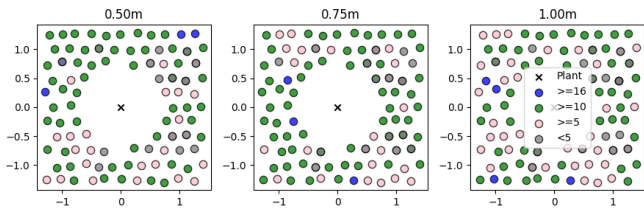


Fig. 2: Colors represent the numbers of visible strawberries from different positions, visualized by circles, in an example environment where a single plant at the center has 24 fruits in total. Heights of 0.50m, 0.75m, and 1.00m were considered.

simulate sequences of active motions of embodied agent in orchards (cf. Fig. 6a–6g). Visual labels—i.e., bounding box and instance segmentation—of every observable fruit (Fig. 1) are also included for research in agricultural active vision.

To the best of our knowledge, DAVIS-Ag is the *first* public dataset purposed to assist in active vision research particularly in agricultural domains. In addition, we present motivating examples to quantify and visualize the impact of occlusions on the levels of fruit visibility in plant environments. Furthermore, we provide experimental results of several baseline models as benchmarks on the task of target visibility maximization, using this dataset. Additionally, transferability to real strawberry environments is tested to examine both visual fidelity and utility for prototyping in real-world applications. To promote future research, our dataset is made publicly available online.

## II. RELATED WORK

### A. Active Vision for Non-Agricultural Applications

Active vision has been broadly studied for decades in robotics [4], and it includes subfields of various tasks, such as classification [12], [13], detection [14], and manipulation [15] of objects, segmentation [16] and reconstruction [17] of scenes, and also searching for certain items in environments [18], [19]. Though objective functions can differ depending on the scenario, the same goal is essentially pursued to optimize the next poses of agent with visual sensors to gain the most useful information for vision tasks.

1) *Table-top Datasets*: T-LESS [20], BigBIRD [21], and ROBI [22] each provide RGB images along with depth data for a single or multiple objects arbitrarily posed on a “turntable” over which cameras were systematically moved along a spherical grid to emulate possible motions of an robotic arm. Single-plant scenarios in DAVIS-Ag are similarly designed to simulate a mobile robot, moving around a target plant located at the center of the field.

2) *Scene Understanding*: Similar to DAVIS-Ag, Active Vision Dataset (AVD) [23] and Real 3D Embodied Dataset (R3ED) [24] both offer not only bounding boxes of objects in each image but the links between densely sampled viewpoints if they are reachable by an application of one of six actions—i.e., forward, backward, left, right, rotate clockwise, and rotate counterclockwise—to simulate an exploratory robot in

	Strawberry	Tomato	Goblet Vine
Plant/Trunk Height	40	100	70
Fruit Radius	2.5	3	0.75
Leaf Length/Width	10	20	18
Camera Altitudes	25, 40, 55	70, 110, 150	50, 75, 100

TABLE I: Top three rows show the default values of parameters for plant generation in Helios, in which the fruit radius of vine refers to that of individual berries. The last row reveals the three camera heights considered for each orchard type. Every value is in units of centimeters.

a scene. Yet, ours includes “vertical” translations such as up and down as well to emulate freer motions in agricultural open fields, which might be particularly useful to avoid occluders through highly complex structures of plant. We also add some level of white noise to the camera positions to account for possible “slips” of robot in unfavorable terrain conditions, while AVD [23] and R3ED [24] do not incorporate this into their indoor navigation.

More recently, photorealistic 3D simulators e.g., Habitat 3.0 [25]) have been introduced to enable virtual embodied agents to interact with physics-engine-based environments which also offer realistic visualizations. As in [26], however, DAVIS-Ag is a pre-computed dataset that includes all possible visuals for spatial exploration, enabling researchers to incorporate them easily into their framework namely on any development environment. Furthermore, while all existing platforms mentioned above were created to visualize indoor environments, DAVIS-Ag is uniquely designed for exploration in agricultural “outdoor” fields with distinct objects, such as fruits, leaves, and stems.

### B. Active Vision in Agriculture

In agriculture, active vision has been investigated to better monitor statuses of plants, localize fruits for robotic picking, or predict potential yields under significantly cluttered environments. For example, dynamic viewpoint-decision systems were developed to strategically move a robotic arm to accurately estimate the maturity [6] or the size [9] of partially visible fruit. In addition, maximizing the viewed area of target fruit has been studied to closely examine the instance as well as provide a manipulator with useful information for picking [5], [9]. For similar motivation, the authors in [10] used active motions of a robotic arm with a sensor to reconstruct the hidden structure of fruit under another object. Full 3D reconstruction of entire plant also has been performed in the context of active vision [8], [27].

Nonetheless, absence of a common testbed—such as ones discussed in Section II-A—has been a challenge to evaluate a method against another in agricultural applications. For instance, most of the employed simulators have been implemented based upon V-REP [28], Panda3D [29], or Robot Operating System (ROS) [30] with Gazebo [31] which are specially customized for each research problem. In this paper, on the other hand, we propose DAVIS-Ag, which does not require technical familiarity with any of those

	Step Size	Heights	Angles	Actions	Images
SP	25cm	3	1	6	285 ~ 348
MP	50cm	2	12	8	1,128 ~ 1,800

TABLE II: Left four columns show the settings for SP and MP scenarios, including the numbers of possible camera altitudes and angles, while the right-most column indicates the number of images per virtual farm in each scenario.

for simulating robot motions, since “view-to-view” pointers, linking reachable view images, are available.

In a similar sense, DAVIS-Ag is distinct from other agricultural datasets, which only provide the images that were gathered independently for traditional computer vision tasks [11], [32], [33]. It is also different from the datasets for localization tasks [34], [35]—generally collected using camera sensors, inertial measurement units, and wheel encoders as mobile robots travel along fixed paths—since their sparse samples do not allow for simulations of novel trajectories.

### III. DATA SYNTHESIS & COLLECTION

This section describes more technical details on our pipeline for simulation and procedure of data collection.

#### A. 3D Plant Simulation

Our data synthesis pipeline is built based upon our simulation toolbox [36], leveraging the AgML<sup>1</sup> and the Helios [37] frameworks. Specifically, AgML is utilized to interface with the Helios plugins, visualizing simulated three-dimensional plants and environments through OpenGL [37]. In particular, these simulation outcomes encompass realistic, diverse shapes of plants generated based on semi-random tree geometries [38]. Specifically, we configured AgML to utilize several useful plugins of Helios as below:

- *Canopy Generator*: Synthesized three kinds of crops, including goblet vines, strawberries, and tomatoes (cf. Fig. 1), varying their sizes of fruit, leaf, and trunk within the ranges of  $\pm 20\%$ ,  $\pm 20\%$ , and  $\pm 15\%$  from the default settings in Table I.
- *Visualizer*: Generated RGB images of  $1280 \times 720$  in resolution from a number of simulated camera positions densely distributed across the field (cf. Section III-B).
- *Synthetic Annotation*: Produced fruit-related labels for each image (cf. Fig. 1b–1d): (1) 2D coordinates of bounding boxes and (2) instance segmentation masks.

#### B. Two-Scale Scenarios & Camera Poses

For each kind of plant, we particularly consider two types of scenarios—i.e., “Single-Plant” (SP) and “Multi-Plant” (MP)—with the camera settings in Table II. Specifically, in SP, each camera view is set up to always aim at the plant at the origin regardless of its spatial position, with a reasonable assumption that tracking a single plant target to

	Strawberry		Tomato		Goblet Vine	
	SP	MP	SP	MP	SP	MP
Scenes	86	77	130	113	182	44
Images	24, 510	86, 856	45, 240	203, 400	63, 336	79, 200

TABLE III: Data size for each type of plant in DAVIS-Ag.

maintain it within the view can be easily implemented. The set of possible actions includes *forward*, *backward*, *left*, and *right* along with *up* and *down*, which control the altitude of viewpoint between three levels specified in Table I.

On the other hand, MP uses three plants in a single row for both tomato and goblet vine cases albeit five in a row for strawberry fields. Additionally, the RGB images are sampled every 30 degrees at each position as in [23], and as a result, *rotate\_clockwise* and *rotate\_counterclockwise* are added to the action set (cf. Fig. 6a–6g). To compensate for this increased computational load in data collection, we set the sampling resolution to be slightly coarser by doubling the step size from 25cm [24] to 50cm and considering only two levels of camera altitudes—i.e., the highest and the lowest.

As in Fig. 2, contrary to existing datasets [23], [24], we use additive white Gaussian noise with a standard deviation of 2.5cm on each  $x, y$ -coordinate of the camera position to simulate a robot “slipping” in harsh terrain conditions of real outdoor environments. Moreover, the spatial sizes of grid in the two scenarios are set up differently—i.e.,  $3\text{m} \times 3\text{m}$  for SP and  $7\text{m} \times 3\text{m}$  for MP—to keep the space to be sufficiently large for exploration while achieving reasonable computational costs for simulation.

#### C. Labels & Potential Applications

The following labels are available for each RGB image:

- **2D bounding boxes & ID’s** for individual fruits (Fig. 1d).
- **Instance segmentation mask** for each fruit (Fig. 1b).
- **Pointers** to other images reachable by an action.
- **Camera pose**, denoted as  $(x, y, z, \psi, \theta)$  on the global coordinate system, where  $(x, y, z)$  represents the position in three-dimensional space while  $\psi$  and  $\theta$  are the yaw and pitch of camera, respectively.

Bounding boxes around observed fruits are generally useful for building fruit detectors for yield estimation [3], robotic picking, or health monitoring. In particular, identifying individual crops [39] could also be developed from the labels of instance ID. Similarly, instance segmentation could also be useful to find the specific examples of occluded fruit so that a robot could learn an active maneuver to lead better views for “fruit coverage” [5], [40], which infers poses or sizes of individual fruits. In addition, the global camera poses may be useful when validating frameworks for “visual localization” [41] in agricultural environments. “Vision-based navigation” could also be investigated with this dataset, building robots to successfully arrive in a queried view, while only relying on camera sensors. Note that all these domains requiring robot motions can be considered due to the availability of the “view-to-view” pointers.

<sup>1</sup><https://github.com/Project-AgML/AgML>

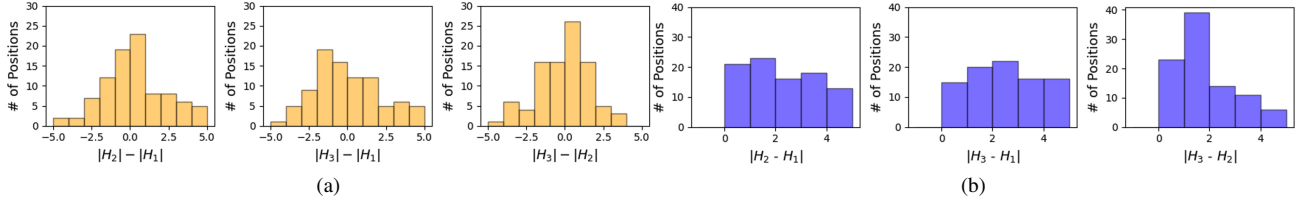


Fig. 3: Histograms depicting (a) the differences in the numbers of strawberries observed at various altitudes and (b) the numbers of newly found instances at higher altitudes.  $H_k$  denotes the set of observable fruits at a particular altitude  $z_k$  at fixed locations within the example of Fig. 2, where  $z_1 < z_2 < z_3$ .

Scenario	Metric	LRD	UDD	Rand	A2C
SP-ST	$OER_\tau$	.433 $\pm .007$	.371 $\pm .008$	.438 $\pm .101$	<b>.520</b> $\pm .004$
	Cum. Reward	.026 $\pm .002$	.008 $\pm .002$	.027 $\pm .002$	<b>.052</b> $\pm .001$
	Ep. Length	2.157 $\pm .043$	2.137 $\pm .036$	2.652 $\pm .056$	<b>2.987</b> $\pm .008$
MP-GV	$OER_\tau$	.316 $\pm .008$	.313 $\pm .006$	.340 $\pm .002$	<b>.369</b> $\pm .009$
	Cum. Reward	.006 $\pm .002$	.004 $\pm .001$	.012 $\pm .002$	<b>.020</b> $\pm .003$
	Ep. Length	2.558 $\pm .097$	2.683 $\pm .118$	4.163 $\pm .058$	<b>5.000</b> $\pm .000$

TABLE IV: Results from evaluated methods on SP-Strawberry (SP-ST) and MP-Goblet Vine (MP-GV) test data. Each average score and standard deviation was computed from three sets of 200 random episodes.

For post-processing, we discarded unreasonably small bounding boxes or ones that barely show a fruit by employing a threshold approach. The minimum numbers of pixels for single strawberries, tomatoes, and grapes were set to 210, 240, and 700, respectively. Additionally, if an action leads to a location either outside the grid or overly close to a plant (e.g.,  $< 75\text{cm}$  for strawberry and  $< 100\text{cm}$  for others), it is regarded as an invalid action, connecting to no image.

#### D. Data Specification

We finally produced  $> 502\text{K}$  images from over 632 virtual farms to construct the DAVIS-Ag dataset. Consequently, our dataset is magnitudes larger than other non-agricultural active vision datasets such as AVD [23] and R3ED [24]. Additional specifications are presented in Table III for further details.

#### IV. MOTIVATING EXAMPLE

Here, we use a representative instance of simulated plant environment to showcase that active viewpoint planning can considerably impact performances in agricultural tasks that would particularly require clear visibility to a certain type of object (e.g., fruit). Specifically, as visualized in Fig. 2, we examined the numbers of visible strawberries from different viewpoints in a field where a single plant with 24 fruits were located at the center of a grid. All configurations for the poses of deployed camera and the environmental settings in this *single-plant* scenario followed the details in Section III-B.

Figure 2 visualizes the dramatic difference in visibility of fruits depending on the camera location; for example, the

number of seeable fruits can significantly vary from  $< 5$  to  $\geq 16$  simply by repositioning the camera only several steps away. In addition, none of the spots provided the viewpoint that can cover all of 24 strawberries at once. Similarly, Fig. 3a proves that even at the same location, using a higher or lower view can also lead to a change to the visibility.

These observations imply that 1) plant environments are essentially highly unstructured, as demonstrated even with this simplified scenario, and thus, 2) the application of *active vision* can greatly benefit autonomous systems for comprehensive monitoring of whole plants or fruits. The latter is particularly advocated by Fig. 3, which shows that though lower views tend to show more strawberries (Fig. 3a), higher ones can still lead to the encounters with novel instances (Fig. 3b). Hence, strategically choosing viewpoints needs to be considered to precisely understand an agricultural environment from perceived information. Our proposed dataset is designed to further encourage relevant research by providing a large amount of realistic plant images with visual and spatial annotations.

#### V. EXPERIMENTAL SETTINGS

##### A. Target Visibility Maximization

Inspired by target area maximization (TAM) [5], which aims to maximize the viewed area of a target object, we define the target visibility maximization (TVM) problem as maximizing the “ratio” of the target fruit’s area to the size of the bounding box at the *last* timestep. Compared to TAM, TVM is designed to avoid incentivizing simplistic motions, such as moving forward to the target, to simply enlarge the target area without reduction of obstruction level. TVM aligns well with sub-tasks intrinsic to robotic harvesting [1] and crop monitoring [2], where robots are not just required to count individual crops but to gain full observations of their surface.

As in other active perception research [23], a target fruit is assumed to be partially visible within the robot’s field of view and localized with a bounding box by a well-trained object detector at the initial timestep. Thus, our focus is on enabling an active agent to plan sequential actions for minimization of the obstruction over the target fruit within the bounding box. For evaluation, we employ the metric “object exposure rate” (OER) after  $\tau$  active motions:

$$OER_\tau \triangleq \frac{n}{(x_2 - x_1)(y_2 - y_1)}, \quad (1)$$

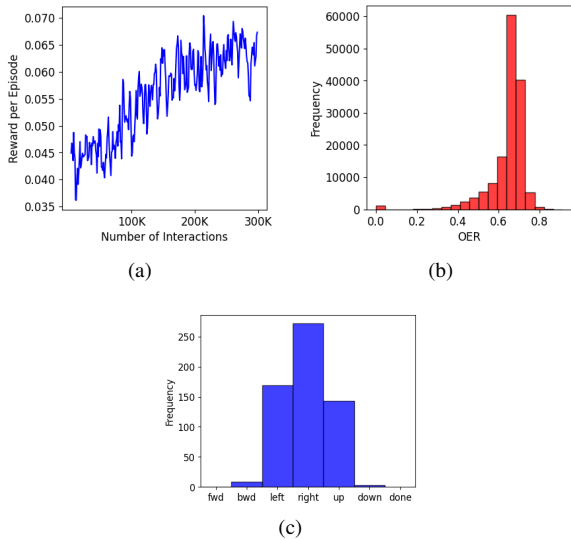


Fig. 4: (a) Episodic rewards over 300K interactions while A2C learns the TVM task from SP-Strawberry data, with some level of rolling average applied for clarity. Frequencies of (b) OER scores for all available strawberry instances and (c) selected actions from tests.

where  $(x_1, y_1)$  represents the upper-left  $x, y$  coordinates, and  $(x_2, y_2)$  the lower-right coordinates after  $\tau$  steps. Here,  $n$  denotes the number of pixels belonging to the target fruit within the bounding box. A higher OER score implies a more unobstructed view of the target object.

### B. Heuristic Baselines

We first consider several heuristic approaches—*LRD*, *UDD*, and *Rand*—selecting a random action  $a_t$  from one of the following action sets  $A$  at each timestep  $t$ :

- $A_{LRD} = \{left, right, done\}$
- $A_{UDD} = \{up, down, done\}$
- $A_{Rand} = \{forward, backward\} \cup A_{LRD} \cup A_{UDD}$

where *done* action is for the robot to decide to stay at the same location and terminate the episode. In the MP scenarios,  $A_{Rand}$  also includes the *rotate cw* and *rotate ccw*.

### C. RL Agent & Implementation

We also train an agent using the Advantage Actor Critic (A2C) reinforcement learning (RL) algorithm [42]. To be specific, at each time  $t$ , the A2C agent decides its action  $a_t$  by processing an input  $\mathcal{X}_t \in \mathbb{R}^{224 \times 224 \times 4}$ , which is obtained by concatenating the downsized RGB image  $\mathcal{I}_t \in \mathbb{R}^{224 \times 224 \times 3}$  from the current viewpoint and the target bounding box  $\mathcal{B}_t \in \mathbb{R}^{224 \times 224 \times 1}$ . In particular,  $\mathcal{B}_t$  is a zero matrix with the values of one inside the bounding box’ area.

This action selection process is iterated  $\tau$  times for an episode, and the sequence of actions is then evaluated based on the final OER. Depending on the quality of obtained views, a reward  $r$  is computed in the following manner:  $r = |\max(OER_\tau - OER_0, 0)|^2$ , where  $OER_t$  denotes *OER* at time  $t$ . That is, the actions leading to an increase

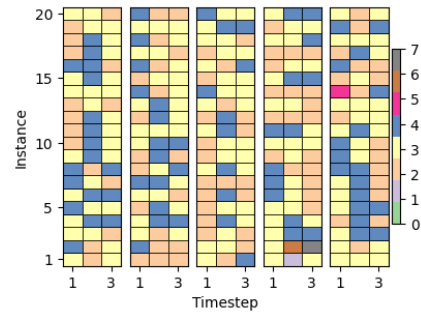


Fig. 5: Action choices in 100 representative test episodes in SP-Strawberry farms. Actions 0 to 6 correspond to *forward*, *backward*, *left*, *right*, *up*, *down*, and *done*, respectively.

Split	Real-Only			DAVIS-Ag $\rightarrow$ Real		
	1	2	3	1	2	3
mAP@50	.943	.888	.920	<b>.945</b>	<b>.911</b>	<b>.936</b>
mAP@50:95	<b>.619</b>	.504	.505	.618	<b>.511</b>	<b>.517</b>

TABLE V: Test performance for ripe strawberry detection under different splits employed out of [43]. The highest value for each split and each metric is in bold.

in the OER are reinforced to cause them to be more likely executed in similar visual states.

The neural network architecture consists of three convolutional layers—i.e.,  $(8, 3)$ ,  $(4, 2)$ , and  $(3, 1)$ , indicating (kernel size, stride)—followed by a fully-connected layer to produce 512-dimensional feature vectors. Additionally, an action network and a value network utilize separate fully-connected layers to generate actions and estimate the state’s value from these features, respectively.

### D. Task Configurations

We explore both SP and MP scenarios to test the active perception capabilities. Specifically, SP of strawberry data is employed for each episode with time steps  $\tau = 3$ , whereas MP involves the data of goblet vines with  $\tau = 5$ . Each episode is terminated when either  $\tau$  steps have been taken or *done* action is executed. Moreover, if the robot acts to move out of the global grid or to a location from which the target fruit is not viewed, that movement is ignored to keep the robot at the previous position. In experiments, the same split is applied to use 70% and 30% data for training and test environments, respectively, unless mentioned otherwise. Each episode is initialized with a random viewpoint showing a target fruit with an OER  $< .400$ . Figure 4b displays the right skewed distribution of OER’s in the SP-Strawberry dataset, with 4% instances satisfying this condition. Note that while each test session involves 200 episodes, the average performance over three independent sessions is reported here.

## VI. RESULTS

Figure 4a displays the increasing trend of the earned reward while the A2C agent performed 300K interactions to learn the TVM task in the SP-Strawberry environments, which eventually took around 90 minutes. Table IV suggests

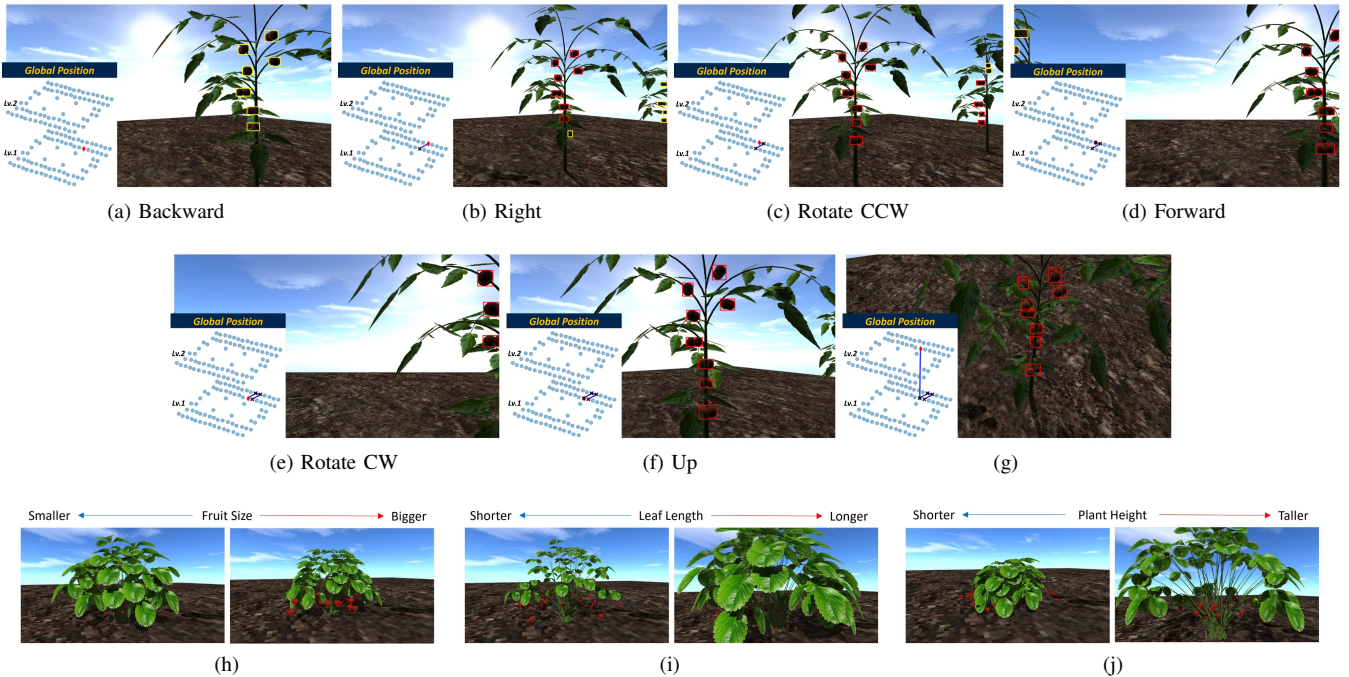


Fig. 6: (a)–(g): Example trajectory from  $t = 0$  to  $t = 6$ , applying six actions in a Multi-Plant Tomato scene. For each RGB image, the caption indicates the action to be taken, and bounding boxes around tomatoes and global locations are also visualized for readers. For instance, the yellow (red) boxes surround unseen (seen) fruits, and the global map shows current positions with red diamonds and the traversed path as the solid line. (h)–(j): Single strawberry environments with various phenotypic characteristics intentionally generated to increase diversity in the dataset.

that there is a strong correlation between the reward and the final OER, supporting the proposed design of reward function. Although the reward for A2C dropped to .052 against the test set of unseen data, it was still significantly higher than the levels that other baseline methods could achieve. Moreover, A2C agent led to over 18% higher OER than other approaches. While the poorest performance of UDD indicates the low utility of the *up* and *down* actions, Fig. 4c reveals that A2C actually learned these “seemingly weak” actions to successfully combine with others. Figure 5 also visualizes the dynamic action choices with diversity.

Table IV shows similar results from the MP Globlet Vines scenarios. Though A2C still offers the best performance, the gap with other baselines has become slightly more marginal, motivating creation of better models to generate reliable longer plans with more options of action in a larger field.

#### A. Real-World Transferability

We also investigate the realism of DAVIS-Ag since our ultimate goal is to assist in prototyping of active vision-enabled autonomous systems in actual plant environments. As a proxy, we follow previous protocols for synthetic datasets [44], designing a ripe strawberry detection problem to test whether the performance is enhanced, if the detector is pre-trained with DAVIS-Ag and fine-tuned with real images.

Specifically, a real strawberry-image dataset collected under natural field/light conditions in [43] was utilized along with the YOLOv5n object detector [45]. We employed three

different random splits—each consisting of 654 and 159 images in training and test sets, respectively—to investigate performance under different compositions of data. For pre-training, 2,565 images from 9 SP-Strawberry environments were employed as a training set, while 570 images from two other environments were used as a validation set.

Table V indicates better performance of transfer learning (DAVIS-Ag  $\rightarrow$  Real) compared to learning solely from the real training data (Real-Only) across most splits. This improvement hints the presence of visual elements shared by DAVIS-Ag and reality, demonstrating the feasibility of using the dataset for real-world prototyping. Yet, further investigations into other crop types (such as tomatoes and grapes), varying growth stages, and additional techniques (e.g., style transfer [46]) may be needed to better warrant minimized sim-to-real gaps.

#### VII. CONCLUSION & FUTURE WORK

We have introduced DAVIS-Ag, which, unlike previous agricultural datasets, features spatially dense image samples connected based on reachability to simulate motions of embodied agents. It provides rich labels, such as bounding boxes and instance segmentation, to assist in learning for not only vision-related tasks but also active motion planning. Experiments evaluated baseline methods and demonstrated the realism of the dataset for prototyping real-world solutions. Our future work includes incorporating 3D data, more plant types, and real robot platforms in larger-scale simulations.

## ACKNOWLEDGEMENT

This work was partially supported by the grants from the NSF (OIA-2134901) and USDA-NIFA (USDA-020-67021-32855).

## REFERENCES

- [1] G. Kootstra, X. Wang, P. M. Blok *et al.*, “Selective harvesting robotics: current research, trends, and future directions,” *Current Robotics Reports*, 2021.
- [2] T. Choi, O. Would, A. Salazar-Gomez, and G. Cielniak, “Self-supervised representation learning for reliable robotic monitoring of fruit anomalies,” in *ICRA*, 2022.
- [3] A. G. Olenskyj, B. S. Sams, Z. Fei *et al.*, “End-to-end deep learning for directly estimating grape yield from ground-based imagery,” *Comput. Electron. Agric.*, 2022.
- [4] R. Bajcsy, “Active perception,” *IEEE*, 1988.
- [5] C. Lehnert, D. Tsai, A. Eriksson, and C. McCool, “3D move to see: Multi-perspective visual servoing towards the next best view within unstructured and occluded environments,” in *IROS*, 2019.
- [6] R. van Essen, B. Harel, G. Kootstra, and Y. Edan, “Dynamic viewpoint selection for sweet pepper maturity classification using online economic decisions,” *Applied Sciences*, 2022.
- [7] T. Zaenker, C. Smitt, C. McCool, and M. Bennewitz, “Viewpoint planning for fruit size and position estimation,” in *IROS*, 2021.
- [8] A. K. Burusa, E. J. van Henten, and G. Kootstra, “Attention-driven active vision for efficient reconstruction of plants and targeted plant parts,” *arXiv*, 2022.
- [9] X. Zeng, T. Zaenker, and M. Bennewitz, “Deep reinforcement learning for next-best-view planning in agricultural applications,” in *ICRA*, 2022.
- [10] R. Menon, T. Zaenker, and M. Bennewitz, “Viewpoint planning based on shape completion for fruit mapping and reconstruction,” *arXiv*, 2022.
- [11] N. Häni, P. Roy, and V. Isler, “Minneapple: a benchmark dataset for apple detection and segmentation,” *IEEE Robotics and Automation Letters*, vol. 5, no. 2, pp. 852–858, 2020.
- [12] J. Yang, Z. Ren, M. Xu, X. Chen, D. J. Crandall, D. Parikh, and D. Batra, “Embodied amodal recognition: Learning to move to perceive objects,” in *Proceedings of the IEEE/CVF International Conference on Computer Vision*, 2019.
- [13] E. Saffronov, N. Piga, M. Colledanchise, and L. Natale, “Active perception for ambiguous objects classification,” in *IROS*, 2021.
- [14] F. Fang, W. Liang, Y. Wu, Q. Xu, and J.-H. Lim, “Self-supervised reinforcement learning for active object detection,” *RA-L*, 2022.
- [15] R. Cheng, A. Agarwal, and K. Fragkiadaki, “Reinforcement learning of active vision for manipulating objects under occlusions,” in *CoRL*, 2018.
- [16] D. Nilsson, A. Pirinen, E. Gärtner, and C. Sminchisescu, “Embodied visual active learning for semantic segmentation,” in *AAAI*, 2021.
- [17] J. Zeng, Y. Li, Y. Ran, S. Li, F. Gao, L. Li, S. He, Q. Ye *et al.*, “Efficient view path planning for autonomous implicit reconstruction,” *arXiv*, 2022.
- [18] X. Ye, Z. Lin, H. Li, S. Zheng, and Y. Yang, “Active object perceiver: Recognition-guided policy learning for object searching on mobile robots,” in *IROS*, 2018.
- [19] J. F. Schmid, M. Lauri, and S. Frintrop, “Explore, approach, and terminate: Evaluating subtasks in active visual object search based on deep reinforcement learning,” in *IROS*, 2019.
- [20] T. Hodan, P. Haluza, Š. Obdržálek, J. Matas, M. Lourakis, and X. Zabulis, “T-LESS: An rgb-d dataset for 6d pose estimation of texture-less objects,” in *WACV*, 2017.
- [21] A. Singh, J. Sha, K. S. Narayan, T. Achim, and P. Abbeel, “Bigbird: A large-scale 3D database of object instances,” in *ICRA*, 2014.
- [22] J. Yang, Y. Gao, D. Li, and S. L. Waslander, “ROBI: A multi-view dataset for reflective objects in robotic bin-picking,” in *IROS*, 2021.
- [23] P. Ammirato, P. Poirson, E. Park, J. Košecká, and A. C. Berg, “A dataset for developing and benchmarking active vision,” in *ICRA*, 2017.
- [24] Q. Zhao, L. Zhang, L. Wu *et al.*, “A real 3D embodied dataset for robotic active visual learning,” *RA-L*, 2022.
- [25] X. Puig, E. Undersander, A. Szot *et al.*, “Habitat 3.0: A co-habitat for humans, avatars and robots,” *arXiv*, 2023.
- [26] W. Ding, N. Majcherczyk, M. Deshpande, X. Qi, D. Zhao, R. Madhivanan, and A. Sen, “Learning to view: Decision transformers for active object detection,” in *ICRA*, 2023.
- [27] J. A. Gibbs, M. P. Pound, A. P. French *et al.*, “Active vision and surface reconstruction for 3D plant shoot modelling,” *TCBB*, 2019.
- [28] E. Rohmer, S. P. Singh, and M. Freese, “V-REP: A versatile and scalable robot simulation framework,” in *IROS*, 2013.
- [29] M. Goslin and M. R. Mine, “The Panda3D graphics engine,” *Computer*, vol. 37, no. 10, pp. 112–114, 2004.
- [30] M. Quigley, K. Conley, B. Gerkey, J. Faust, T. Foote, J. Leibs, R. Wheeler, A. Y. Ng *et al.*, “ROS: an open-source robot operating system,” in *ICRA workshop*, 2009.
- [31] N. Koenig and A. Howard, “Design and use paradigms for gazebo, an open-source multi-robot simulator,” in *IROS*, 2004.
- [32] N. Chebroly, P. Lottes, A. Schaefer *et al.*, “Agricultural robot dataset for plant classification, localization and mapping on sugar beet fields,” *IJRR*, 2017.
- [33] J. Weyler, F. Magistri, E. Marks *et al.*, “Phenobench—a large dataset and benchmarks for semantic image interpretation in the agricultural domain,” *arXiv*, 2023.
- [34] M. Marzoa Tanco, G. Trinidad Barnech, F. Andrade *et al.*, “Magro dataset: A dataset for simultaneous localization and mapping in agricultural environments,” *IJRR*, 2023.
- [35] R. Polvara, S. Molina, I. Hroob *et al.*, “Bacchus long-term (BLT) data set: Acquisition of the agricultural multimodal blt data set with automated robot deployment,” *JFR*, 2023.
- [36] D. Guevara, A. Joshi, P. Raja *et al.*, “An open source simulation toolbox for annotation of images and point clouds in agricultural scenarios,” in *ISVC*, 2023.
- [37] B. N. Bailey, “Helios: A scalable 3D plant and environmental biophysical modeling framework,” *Front. in Plant Sci.*, 2019.
- [38] J. Weber and J. Penn, “Creation and rendering of realistic trees,” in *SIGGRAPH*, 1995.
- [39] R. Kirk, M. Mangan, and G. Cielniak, “Robust counting of soft fruit through occlusions with re-identification,” in *ICVS*, 2021.
- [40] T. Zaenker, C. Lehnert, C. McCool, and M. Bennewitz, “Combining local and global viewpoint planning for fruit coverage,” in *ECMR*, 2021.
- [41] R. Polvara, S. M. Mellado *et al.*, “Collection and evaluation of a long-term 4D agri-robotic dataset,” *arXiv*, 2022.
- [42] V. Mnih, A. P. Badia, M. Mirza, A. Graves, T. Lillicrap, T. Harley, D. Silver, and K. Kavukcuoglu, “Asynchronous methods for deep reinforcement learning,” in *ICML*, 2016.
- [43] M. Lemsalu, V. Bloch, J. Backman, and M. Pastell, “Real-time CNN-based computer vision system for open-field strawberry harvesting robot,” *IFAC-PapersOnLine*, 2022.
- [44] J. Shermeyer, T. Hossler, A. Van Etten *et al.*, “Rareplanes: Synthetic data takes flight,” in *WACV*, 2021.
- [45] G. Jocher, “Yolov5 by ultralytics,” 2020. [Online]. Available: <https://github.com/ultralytics/yolov5>
- [46] F. Magistri, J. Weyler *et al.*, “From one field to another—unsupervised domain adaptation for semantic segmentation in agricultural robotics,” *Comput. Electron. Agric.*, 2023.